Cement & Concrete Composites 34 (2012) 993–1000

Contents lists available at SciVerse ScienceDirect

Cement & Concrete Composites

journal homepage: www.elsevier.com/locate/cemconcomp

X-ray microtomography (μ-CT) to evaluate microstructure of mortars containing low density additions

Marcos Lanzón [a,*], Veerle Cnudde [b], Tim de Kock [b], Jan Dewanckele [b]

[a] Departamento de Arquitectura y Tecnología de la Edificación, ARQ&IDE. Universidad Politécnica de Cartagena, Paseo Alfonso XIII 50, 30203 Cartagena, Spain
[b] Department of Geology and Soil Science, UGCT, Ghent University, Krijgslaan 281/S8, B-9000 Ghent, Belgium

ARTICLE INFO

Article history:
Received 21 February 2012
Received in revised form 19 June 2012
Accepted 20 June 2012
Available online 27 June 2012

Keywords:
Mortars
Microstructure
X-ray microtomography
Porosity
Additions
Capillary water absorption

ABSTRACT

The present paper examines the effect of expanded perlite, expanded glass and cenospheres on cement mortars porosity. The mortars were scanned using X-ray microtomography (μ-CT) and the reconstructed images were treated with the 3D analysis software *Morpho+*. The mortar microstructure was studied in terms of porosity (open, closed and partial porosity) and the *equivalent diameter* of the pores. Porosity was seen to vary greatly, depending on the low density addition and its internal structure. The lowest open porosity was obtained in mortars made with cenospheres, whereas expanded perlite provided the highest open porosity. Capillary water absorption tests carried out to validate the porosity data confirmed that the expanded perlite mortars had the highest absorption. When additional software for voxel data visualization and light microscopy were used to visualize the mortar microstructure, the digital images and thin sections obtained showed good adhesion between the studied additions and the cement paste.

1. Introduction

X-ray microtomography (μ-CT) is a relatively new non-destructive imaging technique, which allows the study of a material's internal microstructure [1]. The main components of the scanner are: an X-ray tube (source of radiation), a rotational stage and a flat panel detector. The scanner acquires multiple 2D X-ray absorption images (often called projections) that are recorded by a detector while the sample rotates. Once the acquisition process is completed, the saved images are reconstructed using a mathematical procedure from hundreds of the acquired projections taken at different angles. The principles of μ-CT and its application to materials characterization has been reported by Landis and Keane [2]. The resolution of the images is expressed in voxels (3D analogy to a pixel) and, after the reconstruction, the acquired 2D slices can be treated with special software for 3D analysis. Phase analysis is one of the most interesting possibilities of μ-CT, since the phases are differentiated from each other by their brightness, which is a function of X-ray absorption [2]. In μ-CT images of typical cement-based materials, the circular dark spots correspond to lower density phases such as air voids within the mortar, whereas the lighter areas correspond to cement or aggregates. The reconstructed images may be visualized with special software to create 3D solids and so sample visualization is used to ascertain qualitative properties representing possible defects inside the studied material.

In the context of building materials, μ-CT has been used to obtain information about cracks in concrete. The reconstructed images can be segmented to separate cracks from the solid constituents of concrete and then the isolated objects are studied to obtain the total volume or surface of the separated objects [3,4]. The microstructure of building stone has been studied by means of μ-CT in combination with 3D special software *Morpho+*. The method has proven to be useful for evaluating stone weathering behavior and crust formation on stone surface and moreover, data on porosity, pore size distribution, grain size and grain orientation can be obtained [5–8]. The technique has been used to study leaching processes in mortars as well as the role of self-healing agents on partial restoration of concrete after cracking [9–11]. In addition, the obtained μ-CT images can be visualized with special software thus resulting in valuable information on the microstructure [8].

Low density additions have a strong influence on essential properties of mortars, such as mechanical strength and capillary water absorption [12–13]. Payá et al. have studied the role of certain lightweight additions, such as fly ash on cement mortars and they monitored the pozzolanic reaction by means of enhanced conductivity measurements [14–18]. However, some frequently used expanded aggregates have been found to be potentially reactive with cement and thus may cause crack formation and expansion processes [19–23]. Therefore, the role of certain lightweight aggregates is not completely understood as they are added to concrete

* Corresponding author.
E-mail address: marcos.lanzon@upct.es (M. Lanzón).

0958-9465/$ - see front matter © 2012 Elsevier Ltd. All rights reserved.
http://dx.doi.org/10.1016/j.cemconcomp.2012.06.011

and mortar formulations. In this way, μ-CT can be used to obtain further information on microstructural features of mortars since the technique provides reliable information and permits additional three-dimensional visualization of the studied samples.

The goal of this paper is to examine the influence of low density additions on the mortar's porosity and microstructure using μ-CT. To do this, mortar porosity was studied by means of special 3D software and additional software for visualization was used to study the microstructure. Thin sections were prepared as a reference method to visualize the samples' microstructure using light microscopy.

2. Materials and methods

2.1. Characterization of low density additions and sample preparation

The particle size distribution of low density additions ranging in size from 0.02 to 2000 μm was studied by laser diffraction using a Mastersizer 2000 analyzer. In laser granulometry *obscuration* is a measure of the amount of light scattered by the sample and the measurements can be affected by the obscuration level. To obtain constant measurements, the low density additions were dispersed in water to provide obscurations of between 10% and 15% using the Hydro G sample dispersion device, which is equipped with a contra-rotating pump, stirrer and ultrasonic treatment to avoid agglomeration. From the measurement of the particle size distribution, various parameters, including D [4,3] (volume mean diameter), d (0.1), d (0.5) and d (0.9), were computed. The size distribution may be derived from d (0.1), d (0.5) and d (0.9), which are defined as the sizes at which 10%, 50% and 90% of the particles are finer than, respectively. The low density additions were examined by SEM using a Hitachi S-3500N microscope equipped with an EDS detector (Brucker AXS). The accelerating voltage and emission current were 4–5 kV and 68 μA, respectively and the images were captured in secondary electron mode. The EDS measurements were carried out at 15 keV.

The mortars were prepared with crushed limestone aggregates (82.80 wt.%), white Portland cement BL II 42.5R (16.50 wt.%), low density additions (0.60 wt.%) and methyl-cellulose (0.1 wt.%), which is a common additive to adjust water retentivity and workability. The low density additions were: expanded perlite, expanded glass and cenospheres (hollow microspheres) and the resulting mortars are termed; M-EP, M-EG and M-CS, respectively. The components were mixed homogeneously with water in two steps using an automatic mixer according to EN 196-1 recommendations [24]. The water percentage was fixed at 21.1 wt.% in all the samples as water has a major influence on the air occluded during the mixing process. The fresh mortars were poured into $4 \times 4 \times 16$ cm prismatic molds and compacted according to the above mentioned standard. After this, the specimens were cured for 48 h at 20 °C, 90% RH and then removed from the molds and stored in a climatic box at 20 ± 1 °C, 65 ± 5% RH to complete the 28 d of curing.

2.2. Analysis of the mortars using high resolution μ-CT

In μ-CT the achievable resolution is limited by the sample size, which makes it necessary to take small sub-samples. The representativeness of the sample is limited by this operation, making a well-considered compromise between resolution and representative sample size necessary, which is in relation with the scales of the structures one wants to look at [25]. In order to obtain an acceptable estimation of the general properties of the material, the samples to be analyzed should be representative of the material itself including its normal spatial variations [26]. Once the curing process was completed, the mortars were cut and drilled to obtain cylindrical cores of 8 mm diameter. The cores were scanned using the in-house scanner developed in the Centre for X-ray Tomography of Ghent University (UGCT) [27]. The scans were made with a transmission type X-ray tube working at 120 kV and 10 W, using a 3 mm thickness aluminum filter to reduce beam-hardening effects by filtering out the tungsten L-lines

Table 1
Granulometric data of the low density additions by laser diffraction analysis.

	D [4,3] (μm)	d (0.1) (μm)	d (0.5) (μm)	d (0.9) (μm)	Span
EP	193.97	24.82	106.73	511.89	4.56
EG	416.72	294.27	404.15	556.16	0.65
CS	119.67	64.74	112.60	187.58	1.09

EP = Expanded perlite; EG = Expanded glass; CS = Cenospheres.

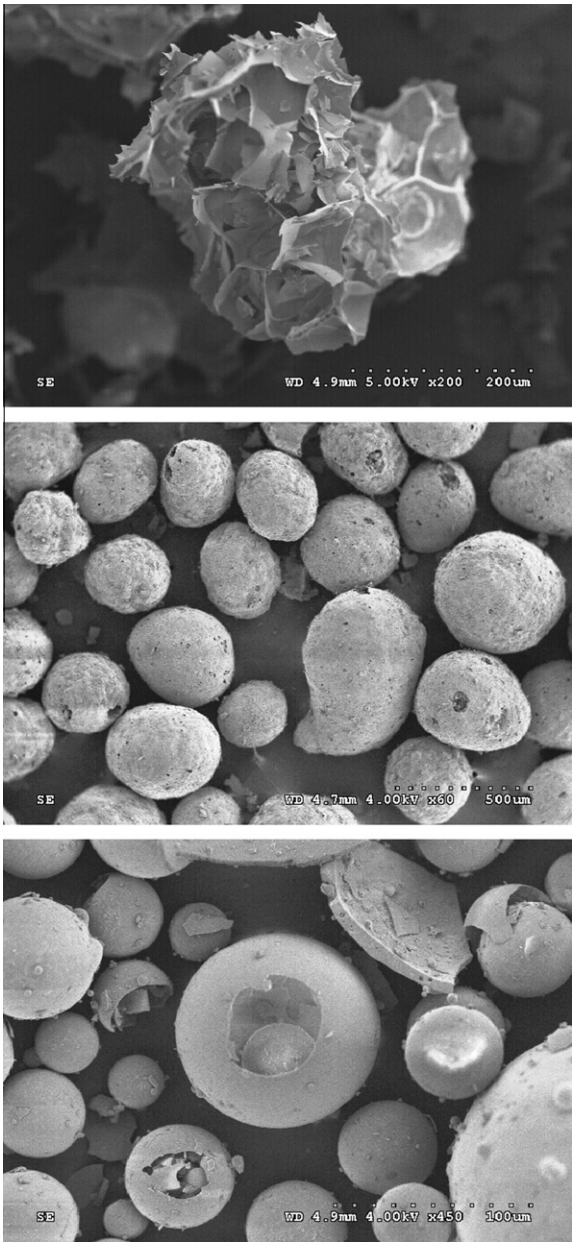

Fig. 1. SEM images showing the morphology of expanded perlite (top); expanded glass (middle) and cenospheres (bottom).

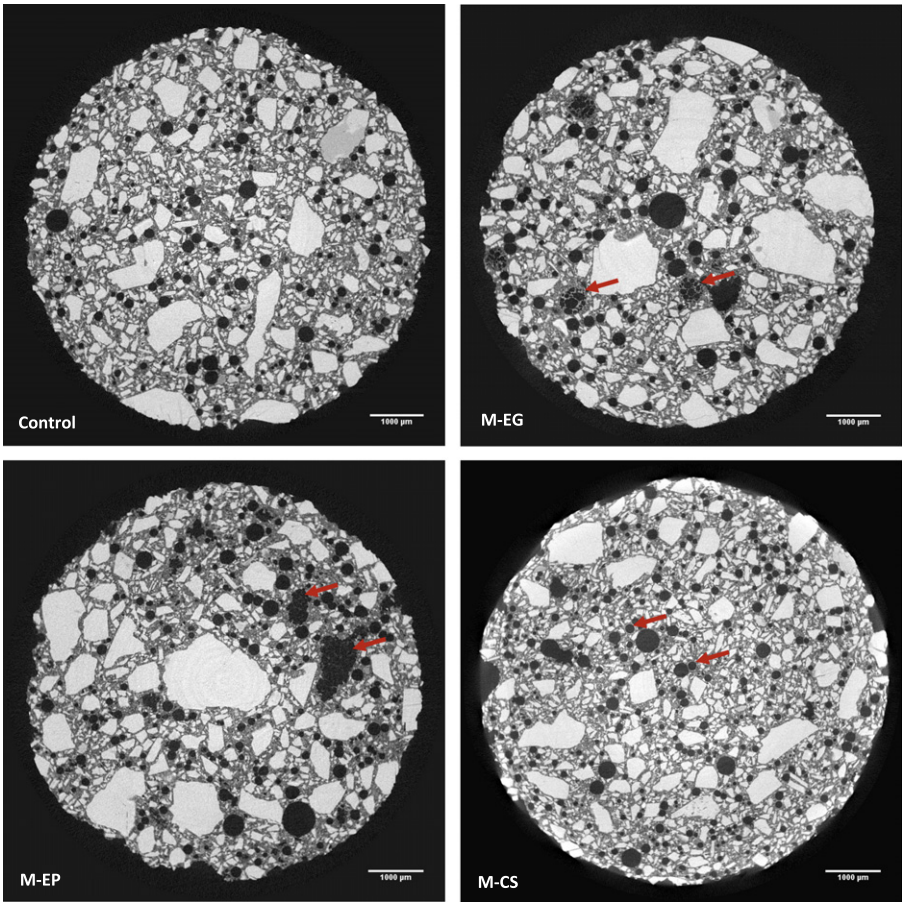

Fig. 2. Sections of images obtained by μ-CT. The arrow shows the location of the low density additions (EP, EG and CS). The length bar at the bottom is 1000 μm.

Table 2
Close, open and total porosity obtained with *Morpho+*.

Sample[a]	Closed porosity (%)	Open porosity (%)	Total porosity (%)	CWA[b] (kg/m^2 min$^{0.5}$)
Control	7.03	1.18	8.21	0.674
M-EP	8.54	3.57	12.11	0.886
M-EG	8.38	1.85	10.23	0.753
M-CS	8.72	0.75	9.47	0.687

[a] M-EP, M-EG and M-CS (mortars containing expanded perlite, expanded glass and cenospheres, respectively).
[b] CWA: Capillary Water Absorption (n = 3).

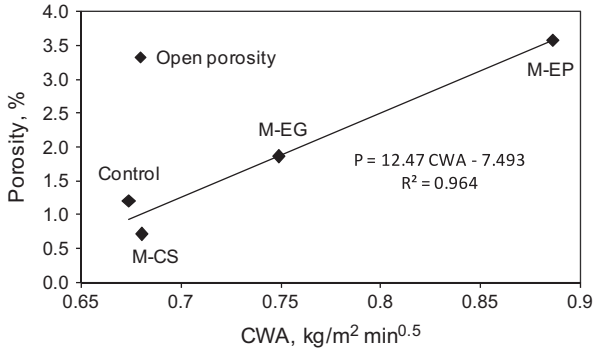

Fig. 3. Correlation found between open porosity and capillary water absorption (CWA).

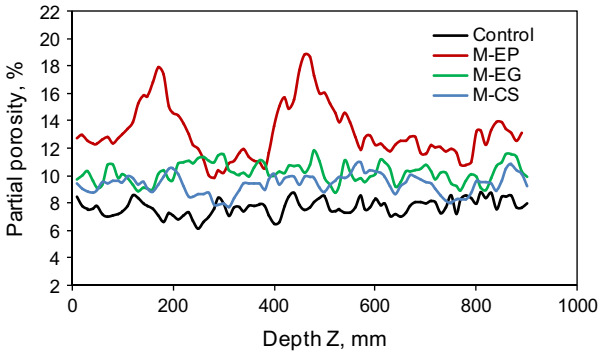

Fig. 4. Partial porosity variation in *Z*-direction.

in the beam and a 6 μm spot size in high power mode. The magnification expressed as the source-detector distance/source-object distance ratio was 50 and the voxel size was 7.93 μm. The sample was placed on a platform rotating 360° with a step of 0.3°. A scintillator 2D panel detector of 2048 × 2048 pixels was used to record the images of the analyzed samples to reconstruct the internal structure. In these conditions, 1200 projections were taken for each sample and the data were reconstructed into μ-CT slices using *Octopus* [6].

2.2.1. 3D analysis of mortars by Morpho+

The reconstructed slices were loaded in *Morpho+* [6,28] to obtain data concerning the 3D microstructure of the mortars, such

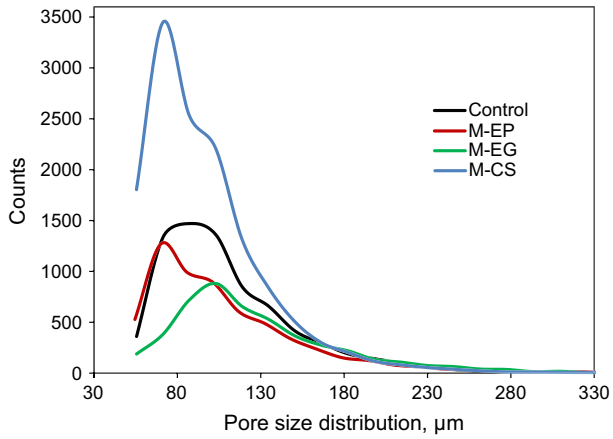

Fig. 5. Number of pores detected of a given size (pore size distribution). The pore sizes were calculated as the equivalent diameter for a spherical representation of pores inside the mortar.

as open and closed porosity, total porosity, partial porosity (% in volume) and equivalent diameter. Partial porosity is defined as the variation of porosity in a longitudinal direction. The volume of interest selected for analysis was segmented in order to separate air pores from solid constituents. To do this the loaded volume was segmented by selecting a certain gray-scale intensity that represents the transition from air to solid phases (threshold). A single threshold operation uses one threshold gray-scale value whereas dual thresholding requires two intervals. In the dual threshold method, voxels with a gray-scale value in the first interval are classified as foreground voxels, while voxels in the second interval are only classified as foreground voxels if they are connected to voxels from the first interval. A dual threshold approach was used in this case as it reduces the sensitivity to residual image noise [28].

Once the air voids were separated, the images were transformed into binary images and labeled. Sample porosity was obtained from the binary volume as a ratio between the volume of pores and the total volume of the sample, including the pores. *Morpho+* uses a routine method (scripting process) to calculate the data, which are automatically saved in a spreadsheet. The same scripting process was applied in all the samples to provide comparable results.

2.3. Microstructure visualization by means of VGStudio and thin sections

The reconstructed images were imported into *VGStudio*. This software allows global or partial visualization of the mortar and its components through segmentation by thresholding the gray-scale intensities of the imported images. As the low density additions provoked substantial differences in pore diameter, the air pores were saved as image files (.bmp) in *Morpho+* and then separately imported into *VGStudio* for visualization.

In addition, individual thin sections obtained from each formulation were prepared to have a reference method and provide more reliable information concerning the microstructure of the samples. The thin sections thus prepared were examined in a *Zeiss Axio*

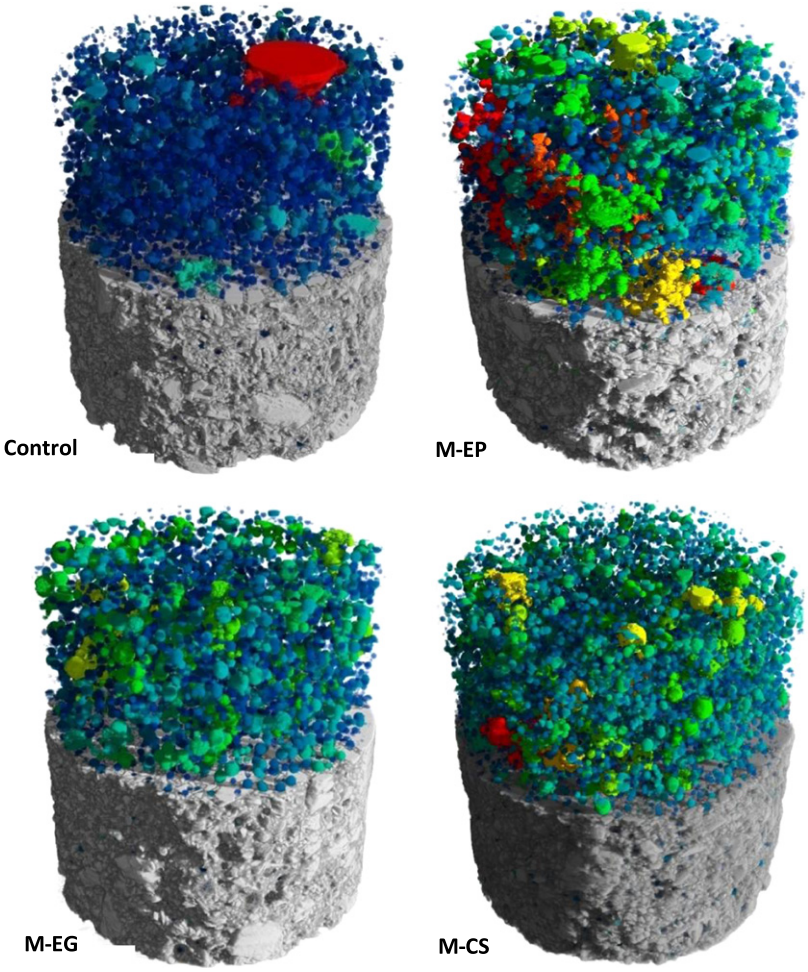

Fig. 6. 3D visualization of mortars by using *VGStudio* (the colored spheres are pores imported from the equivalent diameter data obtained in *Morpho+*).

Scope.A1 petrographic microscope and the corresponding images captured in transmission and reflection mode with a digital camera *AxioCam MRc 5* coupled to the microscope. The microscope was equipped with image processing software *AxioVision 4.8*.

3. Results and discussion

3.1. Study of the low density additions

The laser granulometry results are shown in Table 1. According to the data, the cenospheres had the lowest diameter, whereas expanded perlite and, especially, expanded glass were larger (D [4,3]). The size distribution was the most homogeneous for expanded glass, followed by cenospheres and expanded perlite, both of which showed higher dispersion. The span value, defined as the $[d\,(0.9) - d\,(0.1)]/d\,(0.5)$ ratio, is used to quantify the width of the size distribution in laser granulometry. The narrower the distribution size, the smaller the span becomes. The expanded glass particles were indeed very homogeneous since the span value was very low (0.65). The cenospheres had a narrow distribution as well (1.09) but, in contrast, the size distribution of expanded perlite was the highest (4.56). The morphology of the low density additions was separately studied by SEM to differentiate them from the remaining materials in the mortar images obtained by μ-CT. The internal cavities of expanded perlite are connected with the exterior areas as the perlite is fragile and almost totally hollow (Fig. 1). Expanded glass and cenospheres have external walls with fewer connections with the surrounding area and seem to be more homogeneous in size, as seen in the laser granulometry data (span). Al, Si, and O were the dominant elements, as determined by elemental analysis (EDS).

3.1.1. 3D analysis of the mortars (Morpho+)

The mortars made with the low density additions showed higher porosities than the reference mortar sample (control), as expected (Fig. 2). The low density additions showed good adhesion to the cement paste, as the reconstructed μ-CT images confirm. There are no cracks or discontinuities in the transition zone between expanded perlite, expanded glass or cenospheres and the cement paste. The additions displayed in Fig. 2 show the very thin internal cavities and irregular morphology of expanded perlite particles. Expanded glass seems to be more rounded and partially hollow, whereas cenospheres are not totally closed particles and they are surrounded by thin exterior walls. As can be seen from Fig. 1, the internal pores of the cenospheres can be connected with the

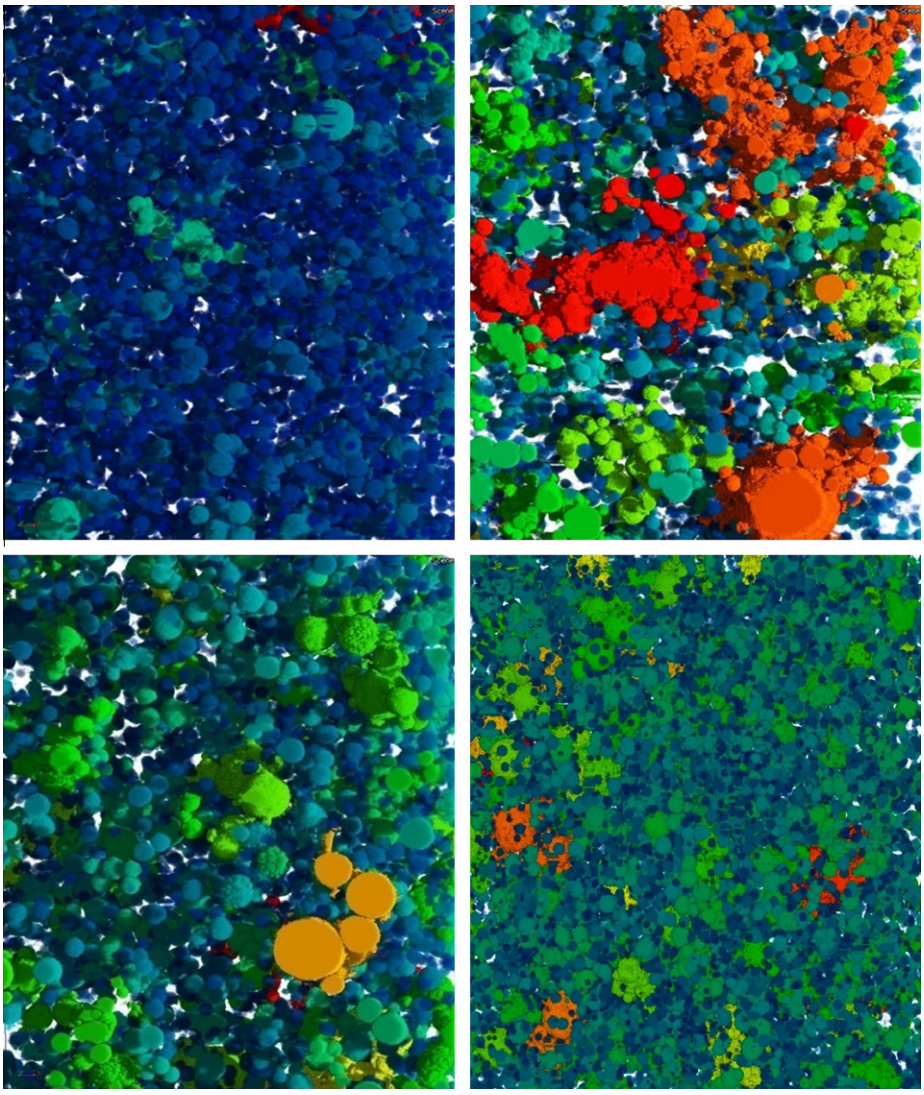

Fig. 7. Air pores (shown as ED) in the samples studied. From left to right and top to bottom: (a) control sample; (b) M-EP; (c) M-EG and (d) M-CS. The largest pores are displayed in red, and the smallest in blue. (For interpretation of the references to color in this figure legend, the reader is referred to the web version of this article.)

exterior areas although to a lower degree than expanded perlite or expanded glass.

The porosity data were obtained after loading the reconstructed images in *Morpho+*. *Closed porosity* is a measurement of the percentage of voxels completely enclosed by material, while open porosity expresses the percentage of voxels belonging to pores which are connected to the surface of the studied volume [28]. The mortars showed similar characteristics in terms of closed porosity, varying from 7.03% to 8.72% (Table 2), meaning that the contribution of the additions in terms of closed porosity was minimal.

Greater differences were found in *open porosity*, with a maximum value of 3.57% for the expanded perlite mortars (M-EP). Open porosity is linked to capillary water absorption since it measures the grade of connection between the internal pores of a mortar and the external surface. Expanded perlite has an open structure (Fig. 1) and the pores of perlite are more connected with the cementitious paste, which is consistent with the M-EP mortar's capillarity (the highest of the three). The capillarity data were obtained by partial immersion of the samples in water [29] to validate the results obtained with *Morpho+* (Table 2). The correlation found between open porosity and capillary water absorption (CWA) is shown in Fig. 3. The relative standard deviation for the capillary water absorption coefficients was determined to be between 1.20% and 4.78% ($n = 3$). Total porosity is calculated as the sum of closed and open porosity.

The porosity results obtained with *Morpho+* are consistent with previous research [13], confirming that M-EP mortars have higher capillary water absorption than M-EG or M-CS mortars. Cenospheres have been found to be pozzolanic in nature [13] so that supplementary cementitious components may be formed around them. For the M-CS mortars, the resulting interfacial transition zone could be denser, with fewer connections between neighboring pores, thus reducing the degree of open porosity.

Partial porosity provides a spatial distribution of the pores inside the sample according to the *X*, *Y* or *Z* axes. The variation in partial porosity (shown in Fig. 4) was calculated in *Morpho+* by dividing the total volume into several subvolumes of 10 slices per step in the *Z*-axis. The mean partial porosity was 7.71%, 13.06%, 10.23% and 9.41% for control, M-EP, M-EG and M-CS mortars, respectively. The fluctuation in partial porosity was calculated from the relative standard deviation RSD % of the data. The M-EP mortars showed the highest fluctuation (17.24%) due to the heterogeneous size distribution of expanded perlite, with the corresponding higher dispersion of pores inside the aggregate. The results are consistent with the laser diffraction data – the narrower the span, the lower the dispersion in partial porosity. The control sample showed lower fluctuations in partial porosity (RSD = 7.38%), whereas M-EG and M-CS showed similar fluctuations to the control sample (7.12% and 7.59%, respectively). Fluctuations in partial porosity may be useful to provide relevant information concerning potential segregation of the low density additions. *Segregation* is defined as separation of constituents of a suspension so that their distribution is no longer uniform. Low density materials, such as expanded perlite, expanded glass or cenospheres are lighter than water and may be separated out because of their lower density, thus producing heterogeneous mixtures. The random fluctuations obtained for M-EG and M-CS mortars are similar to the control sample. The fluctuations obtained for M-EP mortars are probably due to a higher dispersion of the size of the expanded perlite. As partial porosity fluctuates randomly in all the samples, there is no evidence concerning segregation.

Equivalent diameter is defined as the diameter of a sphere with the same volume of the selected pore, and so the parameter gives additional information about the pore size distribution. In the studied samples, a considerable number of pores ranging in size from 60 to 130 μm were found, which were assigned to air voids entrapped during the mixing process and after water evaporation (Fig. 5). The number of small pores found for the M-CS mortars was higher than in the remaining samples since cenospheres have the smallest diameter (D [4,3] = 119.67), which is close in size to the size of the air void pores.

3.2. Microstructure visualization by means of VGStudio and thin sections

The scanned images and pores quantified by equivalent diameter were separately imported to *VGStudio*. As may be seen in Fig. 6, the method permits clear visualization of the mortar constituents (cement, aggregates or low density additions) and pores, which are differentiated by means of their gray scale value, size and/or shape.

Fig. 7 shows the equivalent diameter spherical representation of pores inside each sample. This figure is displayed as a planar section of the pores shown in Fig. 6 and most of the pores arise from air entrapped during the mixing process (air voids). For the M-CS mortars,

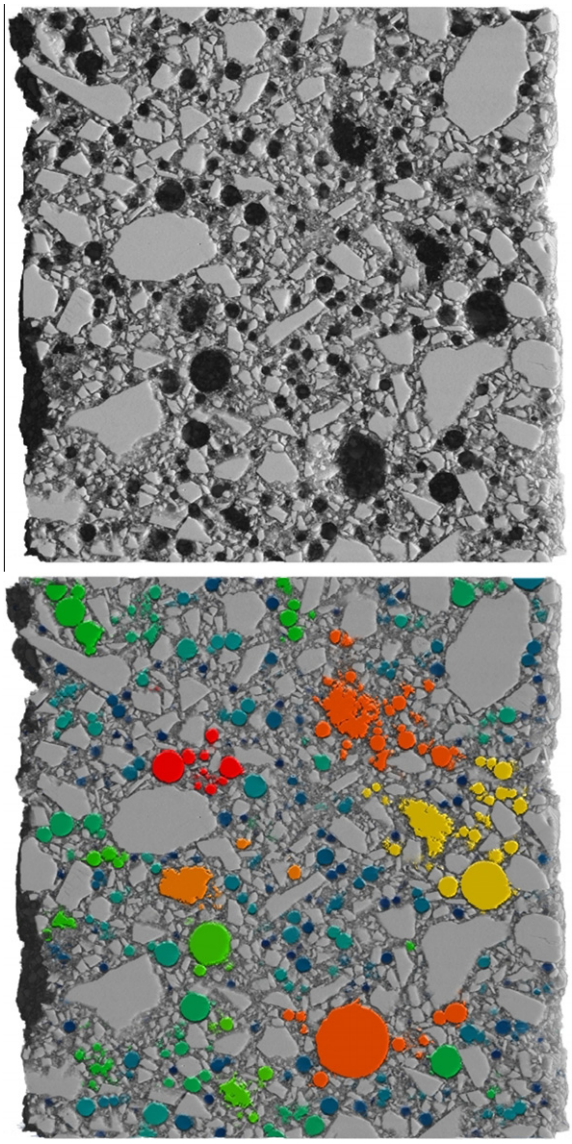

Fig. 8. 2D visualization of M-EP samples. Top: circular pores assigned to air voids are clearly differentiated from irregular pores of expanded perlite. Bottom: images of volume of mortar and pores imported together to *VGStudio*.

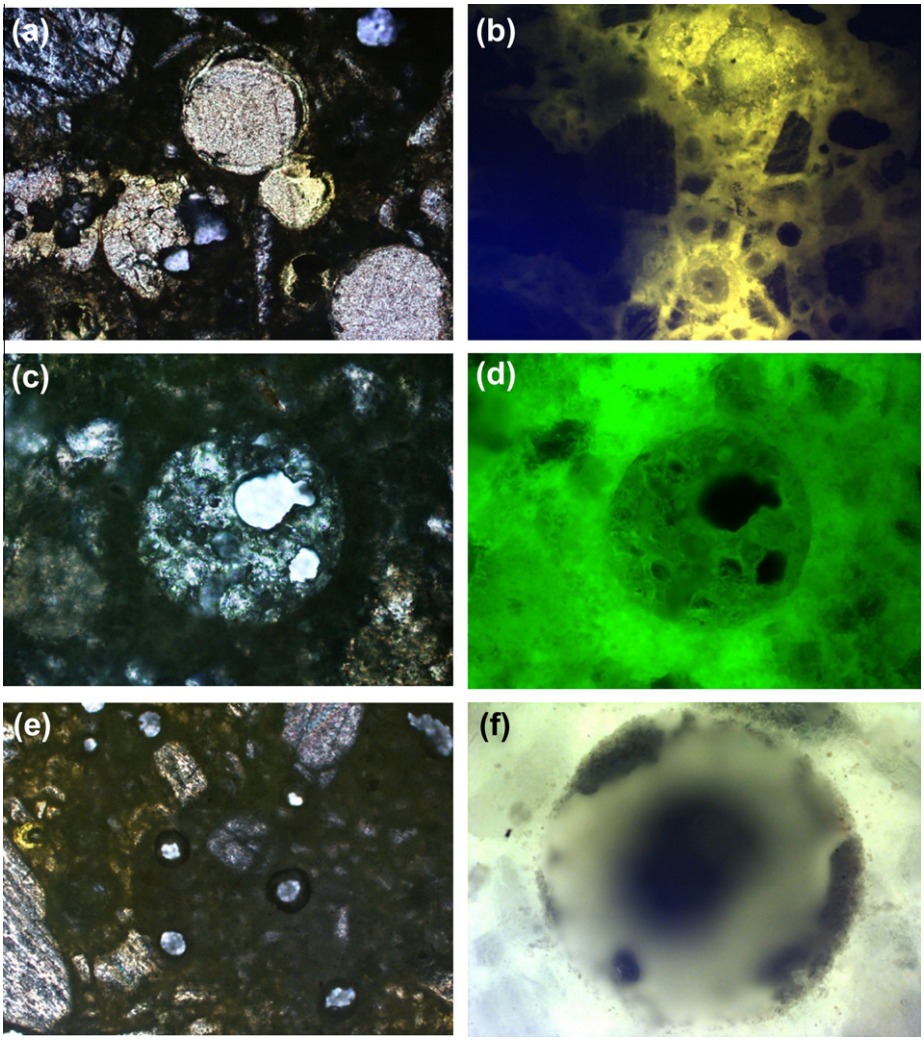

Fig. 9. Thin sections of the mortars carried out at different magnifications: (a) M-EP 10× (transmitted light); (b) M-EP 5× (reflected light); (c) M-EG 20× (transmitted light); (d) M-EG 20× (reflected fluorescent light); (e) M-CS 5× (transmitted light) and (f) M-CS 20× (reflected light).

the pores are again the smallest and least connected compared with the other mortars, confirming the data obtained in Table 2 and Fig. 5. The pores inside M-EP mortars seem to be the largest, as well as the most heterogeneous and interconnected. The interconnection between the pores of M-EP samples provides additional evidence concerning the highest capillarity obtained in the expanded perlite mortars (Table 2). Moreover, the air void pores are clearly differentiated from the pores generated by expanded perlite, as shown Fig. 8. The air void pores (displayed in blue or green) are circular and isolated, whereas the expanded perlite pores (yellow or orange) are irregular and more interconnected.

The mortar microstructures were examined by light microscopy [30] to visualize the compatibility of the low density additions within the cement paste. The thin sections (Fig. 9) provided the same evidence concerning the adhesion of the studied materials with the cement paste, as confirmed by μ-CT (Fig. 2). The thin sections were also examined with reflected fluorescent light and no signs of cracks or discontinuities were found in the transition zone.

The thin sections provide additional information concerning possible interaction between the low density additions and the portlandite of cement. The interfacial zone in the M-EG and M-CS mortars shows evidence of new products (a different phase) formed around the low density additions. These areas are darker in the images captured with transmitted light (Fig. 9c and e), which might be due to chemical reactions between the additions and portlandite. From the reflected light images displayed in Fig. 9d and f, additional evidence of gel formation was found (probably C–S–H) in the transition zone. The thin sections confirm previous research since the transition zone is probably substantially modified by using pozzolanic low density additions [13,31–33].

4. Conclusions and prospectus

The proposed technique needs to be used critically although it has important advantages as compared with other techniques, such as optical microscopy or mercury intrusion porosimetry. In optical microscopy, the thin section preparation requires impregnation and the sample treatment is time-consuming and not easy. In mercury intrusion porosimetry an over-estimation of the open pores can be introduced due to the applied pressure. On the other hand, μ-CT is a non-destructive technique and its combination with special software gives a powerful method as far as time and simplicity are concerned. An obvious limitation in μ-CT is that objects with sizes smaller than the resolution limit are not detected and therefore, the resolution limit is a determining factor as far as the precision of the analysis is considered.

The combination of μ-CT with *Morpho+* permits 3D analyses of mortars containing low density additions. Each mortar's porosity

can be quantified by a simple process consisting of threshold operations, labeling of the objects (pores) and calculation of different types of porosity. The nature of the mortars permits precise segmentation as air is clearly differentiated from the solid components and the low density additions can be clearly observed in the μ-CT images.

Segregation may be studied from the data of partial porosity computed in *Morpho+*. The expanded additions are homogeneously distributed in the mortar as little and random variation in partial porosity was found. The open porosity data obtained with the software were validated with capillary water absorption tests. The results suggest that open porosity could be one of the most important factors in determining capillary water absorption. The software also reports coherent data concerning closed porosity, which was higher in mortars containing cenospheres that are almost hollow particles formed by very thin external walls.

The studied additions are found to bond well to the cement paste because cracks and/or discontinuities were not found. The use of special software for visualization (*VGStudio*) provides a powerful and rapid technique to study the mortar's microstructure. Thin sections obtained by optical microscopy show heterogeneous areas around the expanded glass and cenospheres thus, suggesting a (pozzolanic) reaction between the additions and cement.

A practical conclusion of the paper is that non-usual additions, such as expanded glass or cenospheres can also be used in the manufacturing of lightweight mortar or cement-based materials. Mortars made with expanded glass or cenospheres have lower open porosity and capillary water absorption as compared with mortars containing expanded perlite. Therefore, the additions may have practical application in the manufacturing of mortars and they can be recycled into valuable building materials.

Acknowledgments

The authors express their thanks to the technological service of the Technical University of Cartagena. We are grateful for the samples provided by Cemex España SA, Reverté SA and World Minerals Inc.

References

[1] Baruchel J. X-ray tomography in material science. Paris: Hermes-Science; 2000.
[2] Landis EN, Keane DT. X-ray microtomography (tutorial review). Mater Charact 2010;61:1305–16.
[3] Landis Eric N, Nagy EN, Keane DT, Nagy G. A technique to measure 3D work-of-fracture of concrete in compression. J Eng Mech 1999;125:599–605.
[4] Landis EN, Zhang T, Nagy EN. Cracking, damage and fracture in four dimensions. Mater Struct 2007;40:357–64.
[5] Cnudde V, Silversmit G, Boone M, Dewanckele J, De Samber B, Schoonjans T, et al. Multi-disciplinary characterization of a sandstone surface crust. Sci Total Environ 2009;407:5417–27.
[6] Vlassenbroeck J, Dierick M, Masschaele B, Cnudde V, Van Hoorebeke L, Jacobs P. Software tools for quantification of X-ray microtomography at the UGCT. Nucl Instrum Method A 2007;580:442–5.
[7] Cnudde V, Dewanckele J, Boone M, De Kock T, Boone M, Brabant L, et al. High-resolution X-ray CT for 3D petrography of ferruginous Sandstone for an investigation of building stone decay. Microsc Res Technol 2011;74:1006–17.
[8] Dewanckele J, De Kock T, Boone MA, Cnudde V, Brabant L, Bonne MN, et al. 4D imaging and quantification of pore structure modifications inside natural building stones by means of high resolution X-ray CT. Sci Total Environ 2012;416:436–48.
[9] Burlion N, Bernard D, Chen D. X-ray microtomography: application to microstructure analysis of a cementitious material during leaching process. Cem Concr Res 2006;36:346–57.
[10] Van Tittelboom K, De Belie N, Van Loo D, Jacobs P. Self-healing efficiency of cementitious materials containing tabular capsules filled with a healing agent. Cem Concr Compos 2011;33:497–505.
[11] Van Tittelboom K, Van Loo D, De Belie N, Jacobs P. Evaluation of the efficiency of self-healing in concrete by means of μ-CT. GeoX 2010. Advances in Computed Tomography for Geomaterials, New Orleans, Louisiana, USA; 1–3 March 2010. p. 133–9.
[12] Lanzón M, García-Ruiz PA. Lightweight cement mortars: advantages and inconveniences of expanded perlite and its influence on fresh and hardened state and durability. Const Build Mater 2008;22:1798–806.
[13] Lanzón M, García-Ruiz PA. Lightweight pozzolanic materials used in mortars: evaluation of their influence on density, mechanical strength and water absorption. Cem Concr Compos 2009;31:114–9.
[14] Payá J, Monzó J, Borrachero MV, Peris-Mora E. Mechanical treatment of fly ashes. Part I: Physico-chemical characterization of ground fly ashes. Cem Concr Res 1995;25:1469–79.
[15] Payá J, Monzó J, Borrachero MV, Peris-Mora E, González-López E. Mechanical treatment of fly ashes. Part II: Particle morphologies in ground fly ashes (GFA) and workability of GFA-cement mortars. Cem Concr Res 1996; 26:225–35.
[16] Payá J, Monzó J, Borrachero MV, Peris-Mora E, González-López E. Mechanical treatment of fly ashes. Part III: Studies on strength development of ground fly ashes (GFA) – cement mortars. Cem Concr Res 1997;27:1365–77.
[17] Payá J, Monzó J, Borrachero MV, Peris-Mora E, Amahjour F. Mechanical treatment of fly ashes. Part IV: Strength development of ground fly ash-cement mortars cured at different temperatures. Cem Concr Res 2000;30:543–51.
[18] Payá J, Borrachero MV, Monzó J, Peris-Mora E, Amahjour F. Enhanced conductivity measurements techniques for evaluation of fly ash pozzolanic activity. Cem Concr Res 2001;31:41–9.
[19] Zhang M, Gjorv OE. Microstructure of the interfacial zone between lightweight aggregate and cement paste. Cem Concr Res 1990;20:610–8.
[20] Wasserman R, Bentur A. Interfacial interaction in lightweight aggregate concretes and their influence on the concrete strength. Cem Concr Compos 1996;18:67–76.
[21] Elsharief A, Cohen MD, Olek J. Influence of lightweight aggregates on the microstructure and durability of mortars. Cem Concr Res 2005;35: 1368–76.
[22] Mladenovic A, Suput JS, Ducman V, Skapin AS. Alkali-silica reactivity of some frequently used lightweight aggregates. Cem Concr Res 2004;34:1809–16.
[23] Ducman V, Mladenovic A, Suput JS. Lightweight aggregate base on waste glass and its alkali-silica reactivity. Cem Concr Res 2002;32:223–6.
[24] EN 196-1:1994. Methods of testing cement. Part 1. European committee for standardization.
[25] Gy PM. The sampling of particulate materials – a general theory. Int J Miner Process 1976;3:289–312.
[26] Cnudde V, Boone MN, Dewanckele J, Dierick M, Van Hoorebeke L, Jacobs P. 3D characterization of sandstone by means of X-ray CT. Geosphere 2011;7(1):54–61.
[27] Masschaele BC, Cnudde V, Dierick M, Jacobs P, Van Hoorebeke L, Vlassenbroeck J. UGCT: new X-ray radiography and tomography facility. Nucl Instrum Method Phys Res – Sec A 2007;580:266–9.
[28] Brabant L, Vlassenbroeck J, De Witte Y, Cnudde V, Boone MN, Dewanckele J, Van Hoorebeke L. Three-dimensional analysis of high-resolution X-ray computed tomography data with *Morpho+*. Microsc Microanal 2011;17(2): 252–63.
[29] EN 1015-18:2002. Methods of tests for mortars for masonry. Part 18: determination of water absorption coefficient due to capillary action of hardened mortar. European Committee for Standardization.
[30] Ingham JP. Geomaterials under the microscope. Manson Publishing Ltd.; 2011.
[31] Lilkov V, Djabarov N, Bechev G, Kolev K. Properties and hydration products of lightweight and expansive cements. Part I: Physical and mechanical properties. Cem Concr Res 1999;29:1635–40.
[32] Lilkov V, Djabarov N, Bechev G, Petrov O. Properties and hydration products of lightweight and expansive cements. Part II: Hydration products. Cem Concr Res 1999;29:1641–6.
[33] Hill J, Sharp JH. The mineralogy and microstructure of three composite cements with high replacement levels. Cem Concr Compos 2002;24:191–9.